Ab initio description of domain walls in Permalloy: Energy of formation and resistivities

S. Gallego,[1,2] P. Weinberger,[1] L. Szunyogh,[1,3] P. M. Levy,[4] and C. Sommers[5]

[1]*Center for Computational Materials Science, Technical University of Vienna, Gumpendorferstrasse 1a, A-1060 Vienna, Austria*

[2]*Instituto de Ciencia de Materiales de Madrid, Consejo Superior de Investigaciones Científicas, Cantoblanco, 28049 Madrid, Spain*

[3]*Department of Theoretical Physics and Center for Applied Mathematics and Computational Physics, Budapest University of Technology and Economics, Budafoki út 8., H-1521 Budapest, Hungary*

[4]*Department of Physics, New York University, 4 Washington Place, New York, New York 10003, USA*

[5]*Laboratoire de Physique des Solides, Université de Paris-Sud, 91405 Orsay Cedex, France*

(Received 18 March 2003; revised manuscript received 22 May 2003; published 7 August 2003)

To determine the formation energy and resistivity for domain walls in permalloy (fcc-$Ni_{85}Fe_{15}$) we use the fully relativistic spin-polarized screened Korringa-Kohn-Rostoker method for layered systems and the corresponding Kubo-Greenwood equation in the context of the (inhomogeneous) coherent potential approximation. We find that the difference in formation energy between 90° and 180° domains becomes very small if the domain wall width increases. Furthermore, we show that regardless of the configuration within a domain wall the in-plane components of the resistivity are larger than in a single domain and, in particular, that the anisotropic magnetoresistance ratio within the domain wall vanishes.

DOI: 10.1103/PhysRevB.68.054406 PACS number(s): 75.30.Hx, 73.22.−f, 75.30.Gw

I. INTRODUCTION

Despite recent advances in magnetic imaging the width of domain walls, which is typically only of the order of several hundred Å, not even the best high resolution experiments in domain mapping are able to give reasonably reliable values for the size and magnetic configuration of these walls. Therefore magnetic domains walls and their corresponding electric transport properties still pose substantial experimental and theoretical problems. Very often simple models have to serve to interpret available experimental data on domain walls, in particular in the context of their electrical transport properties; see Refs. 1–9. The first *ab initio* like description and calculation of domain walls was published only very recently;[10] this included a long discussion of the relations between phenomenological and *ab initio* approaches.

Here we will calculate the formation energies of various types of domain walls and their resistivities for permalloy (fcc $Ni_{85}Fe_{15}$) by using, as in Ref. 10, the fully relativistic spin-polarized screened Korringa-Kohn-Rostoker method for layered systems[11] augmented by the (inhomogeneous) single-site coherent potential approximation (CPA).[12] The self-consistent potentials and effective fields correspond to calculations reported in a previous paper[14] and refer to the experimental lattice constant for fcc $Ni_{85}Fe_{15}$.

II. THEORETICAL MODEL

A. Domain walls and their energy of formation

We start by defining the domain wall configurations so as to set the framework for calculating their energy of formation, i.e., the energy to twist the magnetic configuration from its orientation in one domain to the orientation in an adjacent domain. Let $\Delta E[\mathcal{C}_i(L)]$ denote[11] the energy difference of a particular magnetic configuration $\mathcal{C}_i(L)$ of L atomic layers (properly embedded in between two semi-infinite systems) with respect to a given reference configuration $\mathcal{C}_0(L)$,

$$\Delta E[\mathcal{C}_i(L)] = E[\mathcal{C}_i(L)] - E[\mathcal{C}_0(L)], \tag{1}$$

where, when adopting the magnetic force theorem, $E[\mathcal{C}_i(L)]$ and $E[\mathcal{C}_0(L)]$ refer to grand canonical potentials at $T=0$. If c_α^p denotes the respective concentrations of the constituents A and B in layer p, then in terms of the (inhomogeneous) CPA for layered systems[12] $\Delta E[\mathcal{C}_i(L)]$ is given by

$$\Delta E[\mathcal{C}_i(L)] = \sum_{p=1}^{L} \Delta E^p[\mathcal{C}_i(L)] = \sum_{p=1}^{L} \sum_{\alpha=A,B} c_\alpha^p \Delta E_\alpha^p[\mathcal{C}_i(L)], \tag{2}$$

$$E_\alpha^p[\mathcal{C}_i(L)] = \int_{\epsilon_b}^{\epsilon_F} n_\alpha^p[\epsilon;\mathcal{C}_i(L)](\epsilon-\epsilon_F)\,d\epsilon, \tag{3}$$

where the $n_\alpha^p[\epsilon;\mathcal{C}_i(L)]$ are the components of the layerwise projected density of states corresponding to the magnetic configuration $\mathcal{C}_i(L)$, ϵ_b denotes the bottom of the valence band, and ϵ_F is the Fermi energy of the substrate (semi-infinite system). According to the definition given in Eq. (1) $\Delta E[\mathcal{C}_i(L)]>0$ implies that $\mathcal{C}_0(L)$ is the preferred configuration, whereas for $\Delta E[\mathcal{C}_i(L)]<0$, $\mathcal{C}_i(L)$ is preferred.

For the present study of 90° and 180° Bloch walls it is useful to define the following magnetic configurations [$\hat{\mathbf{x}}$ and $\hat{\mathbf{y}}$ refer to the in-plane coordinate vectors, $\hat{\mathbf{z}}$ is normal to the plane (layers)],

$$\mathcal{C}_0(L) = \{\underbrace{\hat{\mathbf{x}},\hat{\mathbf{x}},\ldots,\hat{\mathbf{x}}}_{L}\}, \tag{4}$$

and

$$\mathcal{C}_i(L) \equiv \mathcal{C}_i(L_1;N;L_2;b) = \{\underbrace{\hat{\mathbf{n}}_l,\ldots,\hat{\mathbf{n}}_l}_{b},\hat{\mathbf{n}}_1,\hat{\mathbf{n}}_2,\ldots,\hat{\mathbf{n}}_{L_1},\underbrace{\hat{\mathbf{y}},\ldots,\hat{\mathbf{y}}}_{N},\hat{\mathbf{n}}'_1,\hat{\mathbf{n}}'_2,\ldots,\hat{\mathbf{n}}'_{L_2},\underbrace{\hat{\mathbf{n}}_r,\ldots,\hat{\mathbf{n}}_r}_{b}\}, \tag{5}$$

where $L=N+L_1+L_2+2b$. The orientation of the magnetization in the individual layers $\hat{\mathbf{n}}_k$ is given by

$$\hat{\mathbf{n}}_{k_1}=R(\Theta_{k_1})\hat{\mathbf{x}}, \quad \hat{n}'_{k_2}=R(\Theta'_{k_2})\hat{\mathbf{y}}, \tag{6}$$

where $R(\Theta_{k_1})$ and $R(\Theta'_{k_2})$ are (clockwise) rotations around the axis and $k_{1,2}$ are integers between 1 and $L_{1,2}$. Similar to Ref. 10 we use the simple model of linear Bloch walls, namely,

$$\Theta_{k_1}=k_1\frac{90°}{L_1} \text{ and } \Theta'_{k_2}=k_2\frac{90°}{L_2}. \tag{7}$$

In Eq. (5) the index i denotes different configurations, i.e., different choices of $L_{1,2}$ and N. This set of atomic layers contains b ''buffer layers'' at each end of the wall with orientations $\hat{\mathbf{n}}_l=\hat{\mathbf{x}}$ on the left and $\hat{\mathbf{n}}_r=-\hat{\mathbf{x}}$ or $\hat{\mathbf{n}}_r=\hat{\mathbf{y}}$ on the right. Equation (4) refers to a collinear magnetic configuration with the magnetization oriented uniformly in-plane along $\hat{\mathbf{x}}$. It should be noted that in terms of Eq. (5) noncollinear magnetic structures can be easily defined:[13] in each plane the orientation of the magnetization is uniform (two-dimensional translational symmetry), while the orientation between different planes can vary in an arbitrary manner.

While the magnetic anisotropy energy for bulk $Ni_{85}Fe_{15}$ is very small indeed, it is larger by three orders of magnitude for free surfaces of permalloy;[14] in both cases for a Ni concentration of 85% an in-plane orientation of the magnetization, namely, the configuration defined in Eq. (4), is preferred. Since $\mathcal{C}_0(L)$ refers to the magnetic ground state configuration (uniform in-plane magnetization along $\hat{\mathbf{x}}$, or equivalent to $-\hat{\mathbf{x}}$, $\hat{\mathbf{y}}$ and $-\hat{\mathbf{y}}$) in $Ni_{85}Fe_{15}(100)$ the energy difference defined in Eq. (1) with respect to magnetic configurations of the type given in Eq. (5) can be regarded as the energy of formation for a domain wall; it is a kind of ''twisting energy'' that is needed to form noncollinear structures. It should be noted that in $Ni_{85}Fe_{15}$ a thickness of 1 ML corresponds to about 1.77 Å, i.e., thicknesses given in the following in terms of monolayer are almost twice as large in Å.

As can be seen from Table I we specify different domain wall configurations $\mathcal{C}_i(L)$ by varying N,L_1, and L_2; not only will we consider 90° and 180° domains walls, but by increasing N to a sufficiently large number we can study two 90° domain walls separated from one another. For a 180° domain wall, e.g., the domain wall width is given by $L'=(L-2b)=L_1+L_2$; for a 90° domain wall by L_1.

TABLE I. Different types of Bloch walls considered, $L'=L-2b'$, see Eq. (5).

N	L_1,L_2	Type
0	$L_1=L_2=L'/2$	180° Bloch wall
0	$L_1=L'$, $L_2=0$	90° Bloch wall
$\neq 0$	$L_1=L_2<L'/2$	two 90° Bloch walls

All energy differences in Eq. (1) are evaluated at zero temperature in terms of the magnetic force theorem by integrating in the upper half of the complex energy plane along a contour which starts at a real energy well below the valence band and ends at the Fermi energy. For these calculations a total of 660 $\mathbf{k}_\parallel$ points in the ISBZ is used; as was shown in Ref. 11 in the case of magnetic anisotropy energies this guarantees well converged results. In all calculations the atomic sphere approximation is used; in all angular momentum expansions the maximal quantum number ℓ is two and the parent lattice[13] refers to a fcc-lattice with the experimental lattice constant for $Ni_{85}Fe_{15}$, namely, 6.695 a.u.

B. Domain wall resistivities

We use the Kubo-Greenwood equation for the diagonal ($\mu\mu$th) element of the conductivity tensor for a particular magnetic configuration $\mathcal{C}_i(L)$ of a structure that has only two-dimensional invariance; this is given as[12,15,16]

$$\sigma_{\mu\mu}[L;\mathcal{C}_i(L)]=\lim_{\delta\to 0}\sigma_{\mu\mu}[L;\mathcal{C}_i(L);\delta], \quad \mu\in(x,y,z), \tag{8}$$

where L is the total number of atomic layers considered and δ refers to the imaginary part of the complex Fermi energy $\mathcal{E}_F=E_F+i\delta$. For a current in the plane of the layers (CIP) geometry the corresponding element of the resistivity tensor is defined by[12,15,16]

$$\rho_{\mu\mu}[L;\mathcal{C}_i(L);\delta]=\{\sigma_{\mu\mu}[L;\mathcal{C}_i(L);\delta]\}^{-1}, \tag{9}$$

$$\rho_{\mu\mu}[L;\mathcal{C}_i(L)]=\lim_{\delta\to 0}\rho_{\mu\mu}[L;\mathcal{C}_i(L);\delta]. \tag{10}$$

When the magnetization in all the layers point along the same direction, e.g., along the x axis, [see Eq. (4)], and in the limit of $L\to\infty$, Eq. (10) corresponds to the so-called residual resistivity of a binary substitutional alloys; in principal this can depend on the orientation of the magnetization chosen, i.e.,

$$\lim_{L\to\infty}\{\lim_{\delta\to 0}\rho_{\mu\mu}[L;\mathcal{C}_0(L);\delta]\}=\rho^0_{\mu\mu}(\mathcal{C}_0). \tag{11}$$

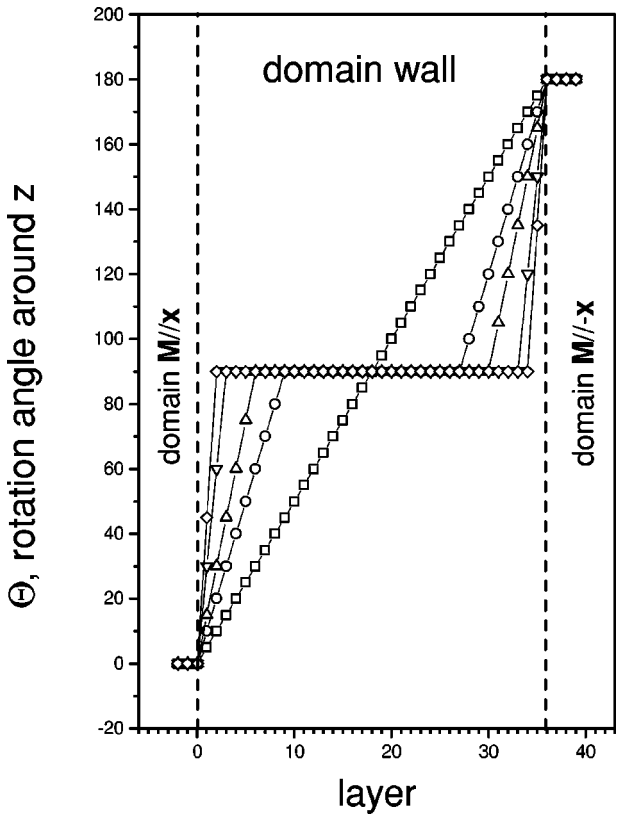

FIG. 1. Sketch of the angular profile keeping $L'=L-2b$, see text, fixed to 36 ML. Squares: $L_1=L_2=18$, $N=0$; circles: $L_1=L_2=9$, $N=18$; up-triangle: $L_1=L_2=6$, $N=24$; down-triangles: $L_1=L_2=3$, $N=30$, diamonds: $L_1=L_2=2$, $N=32$. Shown is the rotation angle around $\hat{\mathbf{z}}$ in each layer.

For example, for $\mathcal{C}_0(L)=\{\hat{\mathbf{n}}_i|\hat{\mathbf{n}}_i=\hat{\mathbf{z}};1\leqslant i\leqslant L\}$ we find

$$\rho^0_{xx}(\mathcal{C}_0)=\rho^0_{yy}(\mathcal{C}_0)\neq\rho^0_{zz}(\mathcal{C}_0), \tag{12}$$

while for $\hat{\mathbf{n}}_i=\hat{\mathbf{x}}$,

$$\rho^0_{xx}(\mathcal{C}_0)\neq\rho^0_{yy}(\mathcal{C}_0)=\rho^0_{zz}(\mathcal{C}_0). \tag{13}$$

By taking $\mathcal{C}_0(L)=\{\hat{\mathbf{x}},\ldots,\hat{\mathbf{x}}\}$, see Eq. (4), we define the anisotropic magnetoresistance (AMR) ratio $R(L)$ in terms of the diagonal elements of the resistivity parallel and perpendicular to the chosen uniform orientation of the magnetization, e.g., by the following ratio:

$$R(L)=\frac{\rho_{xx}[\mathcal{C}_0(L)]-\rho_{yy}[\mathcal{C}_0(L)]}{\rho_{xx}[\mathcal{C}_0(L)]}. \tag{14}$$

In dealing with bulklike cubic systems [see Eq. (4)],[17] the denominator in Eq. (14) is usually replaced by

$$\lim_{L\to\infty}\rho_{av}[\mathcal{C}_0(L)]=\frac{1}{3}\lim_{L\to\infty}\{\rho_{\parallel}[\mathcal{C}_0(L)]+2\rho_{\perp}[\mathcal{C}_0(L)]\}, \tag{15}$$

and the AMR is defined by

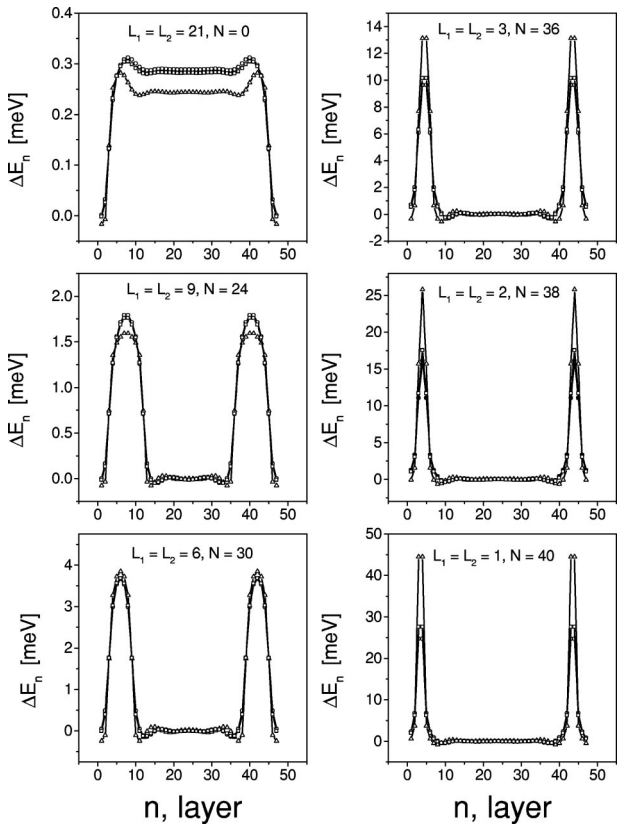

FIG. 2. Layer- and component-resolved interlayer exchange or twisting energy for $L=42$ ML. The various cases of L_1,L_2, and N are indicated. Note that the first and last three layers refer to buffer layers. Circles and triangles refer to Ni and Fe, respectively, and squares to the average.

$$R=\lim_{L\to\infty}\frac{\rho_{xx}[\mathcal{C}_0(L)]-\rho_{yy}[\mathcal{C}_0(L)]}{\rho_{av}[\mathcal{C}_0(L)]}=\frac{\rho_{\parallel}-\rho_{\perp}}{\rho_{av}}. \tag{16}$$

In analogy with Eq. (14) one can define an anisotropic magnetoresistance for non-collinear structures as

$$R[\mathcal{C}_i(L)]=\frac{\rho_{xx}[\mathcal{C}_i(L)]-\rho_{yy}[\mathcal{C}_i(L)]}{\rho_{xx}[\mathcal{C}_i(L)]}, \tag{17}$$

where $\mathcal{C}_i(L)$ is now a magnetic configuration as given in Eq. (5). In particular these ρ_{xx},ρ_{yy}, and $R[\mathcal{C}_i(L)]$ characterize the electrical transport properties of domain walls in the case of the CIP.

In the present calculations the surface-Brillouin-zone integrals needed in the evaluation of the electrical conductivity within the Kubo-Greenwood approach[12] were obtained by considering 1830 $\mathbf{k}_{\parallel}$ points in the irreducible wedge of the surface Brillouin zone. All scattering channels up to and including $\ell_{\max}=2$ were taken into account. The diagonal components of the conductivity tensor were evaluated for finite values of δ [see Eq. (8)], and then numerically extrapolated (continued) to the real energy axis.

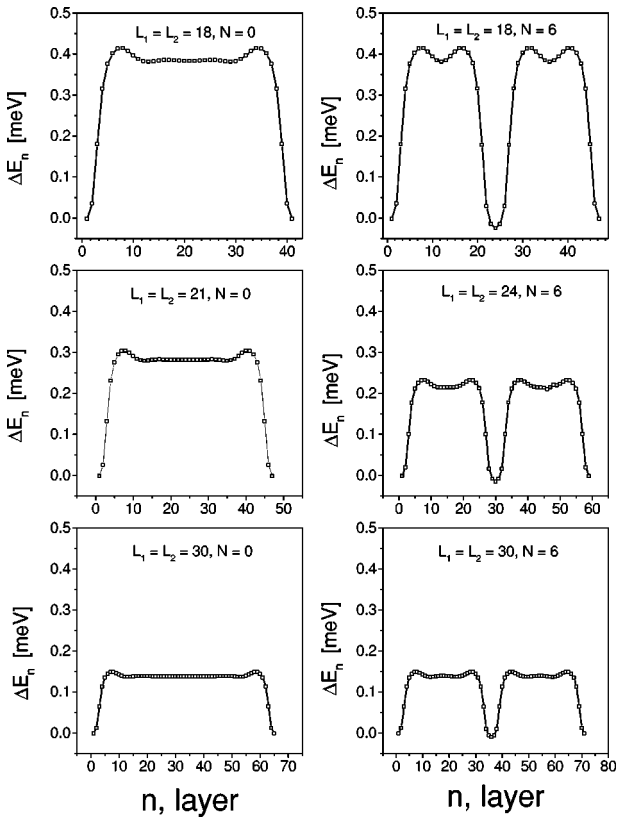

FIG. 3. Layer-resolved interlayer exchange or twisting energy for growing values of L. The various cases of L_1, L_2, and N are indicated. Note that the first and last three layers are the buffer layers.

III. RESULTS

In Fig. 1 we sketch the noncollinear configurations in Eq. (5) for $L=36$. For example, $L_1=L_2=18$ depicts a 180° domain wall in which the magnetization rotates 5° between adjacent layers; while for $L_1=L_2=9$, and $N=18$ there are two 90° domain walls each 9 ML wide that are separated by 18 atomic layers oriented along the $\hat{\mathbf{y}}$ axis ($\Theta_{k_1}=90°$, $\Theta'_{k_2}=0$). While for the first case there is a gradual and uniform rotation in all other cases we consider the rotation varies faster in discrete regions of the wall, and the magnetization points along $\hat{\mathbf{y}}$ in the remainder of the atomic layers.

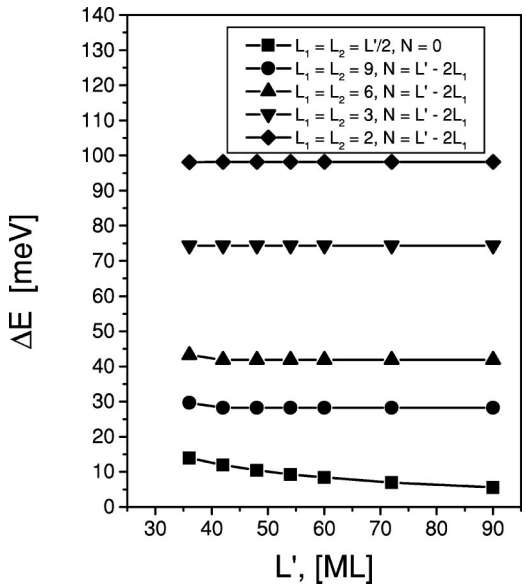

FIG. 4. Domain wall formation energy with respect to $L'=L-2b$; see the text.

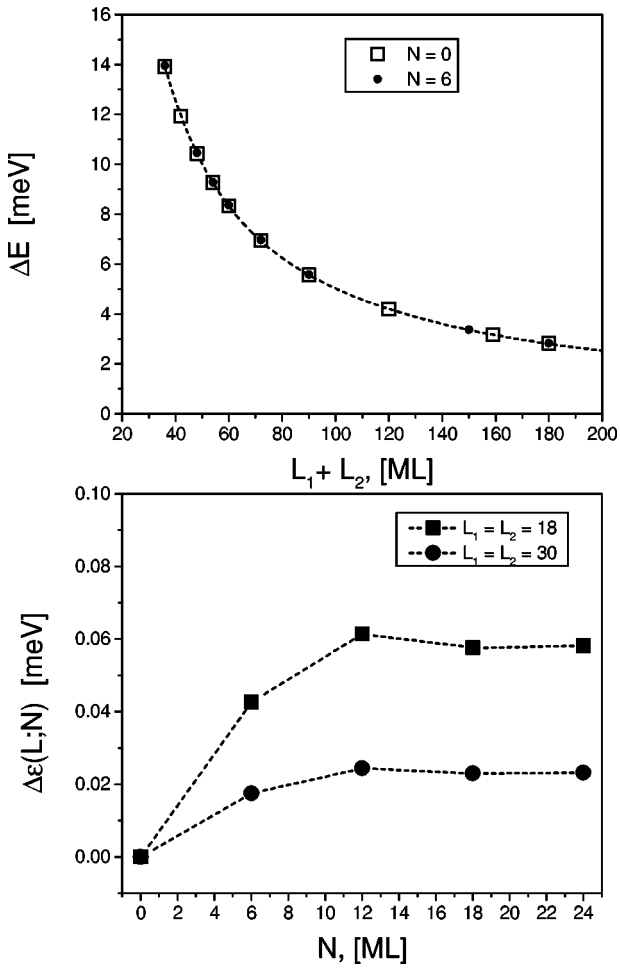

FIG. 5. Top: Energy of domain wall formation as a function of L_1+L_2, see Eqs. (1) and (5). Bottom: Difference in energy between a single 180° domain wall and when this wall is split into two by inserting a domain of N ML that has its magnetization pointing at 90° to the two outer domains, see Eq. (18).

For the discussion below of the energy of domain wall formation it should be recalled that in principle all quantities are evaluated at zero temperature; to reach magnetic configurations corresponding to a $\Delta E[\mathcal{C}_i(L)]>0$ the temperature has to be finite (150 K correspond to about 14 meV).

A. Formation energies

To illustrate the characteristic energy changes caused by changing the profile of the rotation angles Θ and Θ' the layer-resolved twisting energies (band energy differences), see Eq. (2), are useful. In Figs. 2 and 3 two typical cases are shown, namely, (1) keeping L constant and varying N and (2) keeping N constant and varying L.

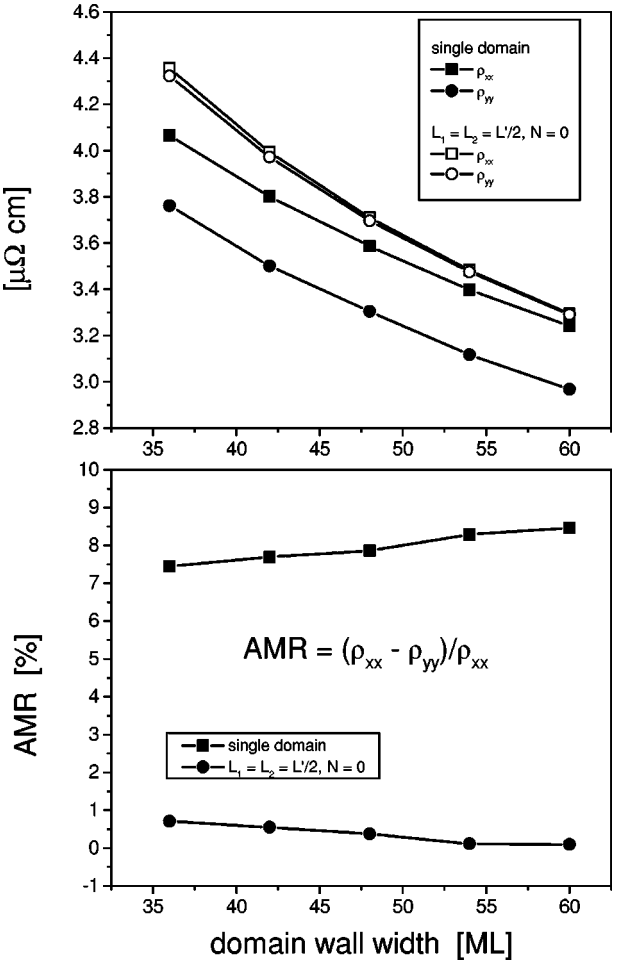

FIG. 6. Comparison of resistivities (top) and AMR (bottom) for a single domain (full symbols) and a 180° domain wall.

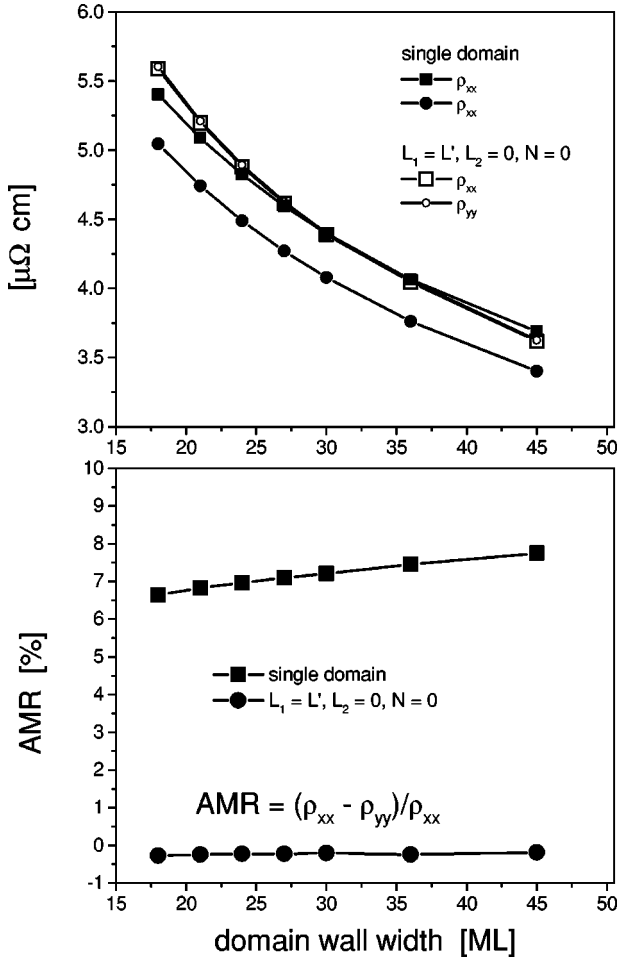

FIG. 7. Comparison of resistivities (top) and AMR (bottom) for a single domain (full symbols) and a 90° domain wall.

In Fig. 2 the situation for $L=42$ is displayed. From this figure one can see, quite impressively, that (1) by increasing N increasingly thinner domain walls between 90° domains are formed and (2) that indeed those layers in which the orientation of the magnetization is along $\hat{\mathbf{y}}$ do not contribute to the total twisting energy (the directions $\hat{\mathbf{x}}$ and $\hat{\mathbf{y}}$ are equivalent). However, one can see another perhaps unanticipated effect; as the domain walls become thinner the Fe-like contribution to the twisting energy increases drastically: when the domain wall is 1 ML thick the Fe contributions are almost twice as large as the Ni contribution. Clearly enough such small domain walls are unrealistic, i.e., only academic; however, these cases show in dramatic terms what happens if the domain walls in permalloy shrink.

In Fig. 3 the opposite behavior is illustrated by keeping N constant and varying $L_1=L_2$. Again one sees that in both cases displayed, namely $N=0$ and 6, the form of the domain walls are unchanged as $L_1=L_2$ is increased and N is held constant. Note that in Figs. 2 and 3 the contributions only from the first 3 ML buffer layers at each end are shown, since for further buffer layers these contributions rapidly vanish. In the semi-infinite bulk part of the systems under investigation they have to be exactly zero. This is the very reason of why it is so important to include a sufficient number of buffer layers: the transition from the walls into the bulk (domains) has to be as smoothly as possible.

As seen from the changing scales for the different entries in Fig. 2 the twisting energy rises sharply with decreasing thickness of the domain wall. Beyond $N=6$ the layers oriented along $\hat{\mathbf{y}}$ do not contribute to the twisting energy. This behavior is summarized in Fig. 4, where we note that for fixed $L_1=L_2$ increasing L does not change ΔE appreciably.

In the upper part of Fig. 5 we show the smallest twisting energies for 90° and 180° domain walls, namely, those referring to the linear variation of the rotation angles; see Fig. 1. The dashed line in Fig. 5 serves as guide to the eye. It is interesting to note that on the scale shown in this figure there is virtually no difference in the formation energies of two 90° or one 180° domain walls provided the total length is the same. It should be noted that in this figure L ranges from $\sim$60 to $\sim$320 Å. In the lower half of Fig. 5 we address an interesting situation; namely the energy needed to split a 180° domain wall in two by inserting a domain of thickness N oriented perpendicular to the outer domains. We define the energy of formation for two 90° domains in a 180° domain wall as

$$\Delta\varepsilon(L;N)=\Delta E[\mathcal{C}_i(L_1;N;L_2;b)]-\Delta E[\mathcal{C}_i(L_1;0;L_2;b')], \tag{18}$$

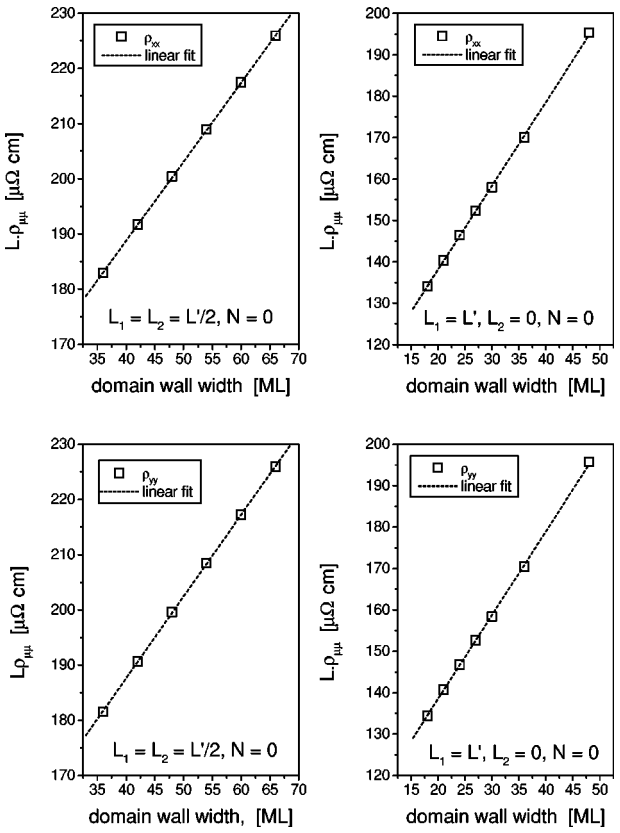

FIG. 8. Thickness dependence of domain wall resistivities for 180° (left column) and 90° (right column) walls, $L=L_1+L_2+2b$.

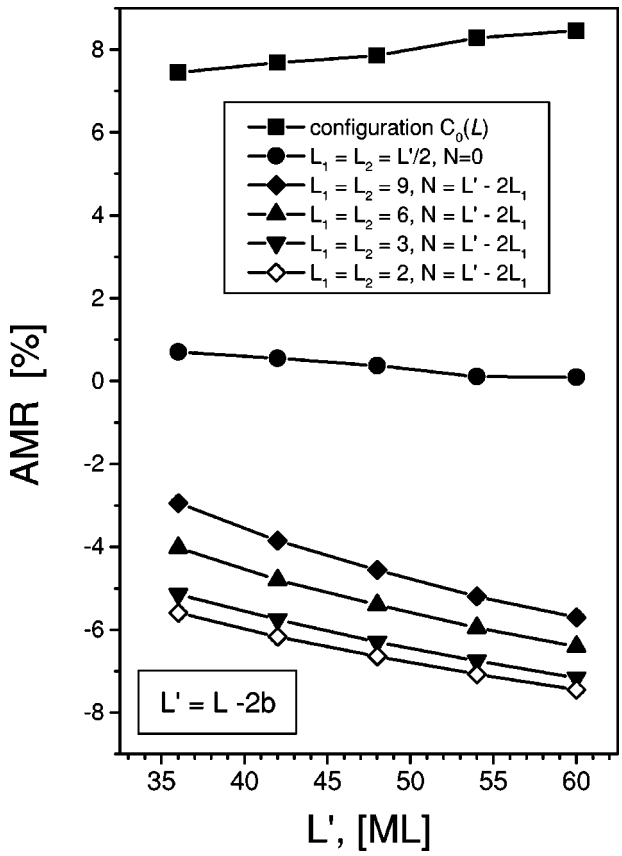

FIG. 9. The AMR as a function of $L'=L-2b$ (see the text) for a 180° domain wall and for two 90° walls separated by N ML whose magnetization is perpendicular to the outer domains. As the separation N between the 90° walls increases the AMR changes sign, going from positive to negative.

and see from Fig. 5 that for

$$L=L_1+L_2+N+2b=L_1+L_2+2b', \tag{19}$$

this quantity is indeed very small and, furthermore, for $N>6$ remains constant, i.e., we find that in permalloy a 180° wall may easily fractionate into two 90° walls. It will be shown in the following section that at least in the investigated case of CIP the actual width of the domain wall is of little importance for the resistivities and the AMR within the wall.

B. Domain wall resistivities

In the upper part of Fig. 6 we show the resistivities as a function of L for a single domain [corresponding to the magnetic configuration in Eq. (4), i.e., for a single (infinite) domain with an in-plane orientation of the magnetization], and for a 180° domain wall. As can be easily seen, not only are ρ_{xx} and ρ_{yy} quite a bit larger in a 180° wall compared to that for a domain, but they are also almost equal in magnitude. As shown in the lower part of this figure the AMR in the domain wall almost vanishes. The same situation applies to a 90° domain wall; see Fig. 7. It should be noted that in Figs. 6 and 7 different scales for the domain wall widths are used. As in all previous cases, see for example the discussion in Ref. 15, beyond a sufficiently large value of L the resistivities ρ_{xx} and ρ_{yy} are linear in L (see Fig. 8), i.e., they can be easily extrapolated to the experimental domain wall widths.

An interesting question to be addressed is the evolution or splitting of a 180° domain wall into two 90° domain walls. This is shown in Fig. 9 by considering prototypes of walls of width $L'=L-2b=2L_1+N$ with varying L' and N. As to be expected for an increasing number of layers oriented along $\hat{\mathbf{y}}$ (N) the ρ_{yy} component increases while ρ_{xx} decreases; this is the origin of the change in sign of the CIP-AMR.

IV. REVIEW OF EXPERIMENTAL DATA

In Ref. 3 a NiFe wire (thickness: 200 Å; width: 1 μm; length: 300 μm) with CoSm pads was investigated (a) in the presence of a repetition of $2N$180° domain walls and (b) in the absence of domain walls. It was found that the difference in resistance between these two cases is independent of temperature and decreases linearly with the number of domain walls. From this linear behavior the authors estimated the domain wall width to be about 1 μm and suggested that " . . . the observed decrease in magnetoresistance can be explained by the AMR effect in the domain walls."

By using zigzag wires the normalized magnetoresistance in $Ni_{80}Fe_{20}$ presented in Ref. 9 is also nearly independent of temperature and amounts to about 0.1%. These authors find a

difference of about -0.08×10^{-6} Ωcm between a multidomain and a single domain resistivity (59.665×10^{-6} Ω cm). In Ref. 4 the same group of authors use the semi-empirical formulas given by Comstock[18] to suggest that the actual film thickness is of quite some importance for the domain wall magnetoresistance. For film thicknesses of 20, 40, and 100 nm they quoted Bloch wall thicknesses of 10, 20, and 50 nm, while for *bulk* permalloy their domain wall width is estimated to be 2000 nm. This latter thickness seems to be rather large.

A decrease in resistance in the presence of domain walls, this time in terms of a nanocontact between two NiFe wires, is reported in Ref. 5 together with an ''AMR ratio'' of -1.1% if the magnetic field is applied transverse to the wire axis and in the plane of the sample.

The very special sample arrangements used in these experimental findings, in particular the reported resistivity (or resistance) values, do not allow us to make direct comparisons to the calculations we made. Most of the experimental papers mention the ''AMR effect,'' and the reduction of resistivities due to this effect. Despite the different experimental set ups used all the above quoted experimental investigations do indicate surprisingly large domain wall widths and rather small AMR values (about 1%) for permalloy. These findings corroborate the present theoretical calculations, i.e., in the case of 180° and 90° domain walls the AMR within the domain wall is close to zero.

V. CONCLUSION

We have presented a fully relativistic *ab initio* calculations for the formation energy and resistivities of domain walls in permalloy ($Ni_{85}Fe_{15}$). The main results of this study can be summarized as follows.

(1) In 90° as well as in 180° domain walls the most likely magnetic configuration corresponds to a linear increase of the rotation angle between adjacent layers; see Table I.

(2) In the domain walls the components of the resistivity tensor parallel and perpendicular to the orientation of the magnetization are slightly larger than in a single domain. In both types of domain walls the anisotropic magnetoresistance nearly vanishes.

(3) As the energy of formation (twisting energy) and the domain wall resistivities are defined with respect to one and the same given noncollinear magnetic configuration a consistent description of both quantities has been given.

Inasmuch as the AMR is used as the underlying physical phenomenon for recording it can be concluded that in the presence of domains walls the AMR active parts in permalloy are confined to the interiors of domains, i.e., the AMR in the walls is negligible. As the energy differences between the 180° and two fractionated 90° walls is small we anticipate that at room temperature permalloy has walls that fluctuate between these two possibilities. Therefore, when a 180° domain wall splits into a sequence of 90° domain walls its AMR fluctuates between positive and negative values (see Fig. 9) for the CIP geometry we considered; this would definitely limit the use of permalloy in sensor applications at room temperature if one used this geometry. In other words one should be sure to design AMR sensors using permalloy so as to avoid this CIP geometry in which fluctuations in the wall can change the AMR, e.g., if one drives the current perpendicular to the plane of the layers then the fluctuations in the pattern of the walls we found would not affect the AMR in this direction. Finally, with respect to the AMR it seems to be irrelevant whether one has a 90° or 180° domain wall; fortunately for its applications to devices the AMR from the walls simply vanishes.

From a purely theoretical standpoint of view it should be recalled that domain walls are manifestations of noncollinear magnetism and as such should be treated in an appropriate manner; the simplest well-defined way consists of assuming noncollinearity in the context of two-dimensional translational symmetry.

ACKNOWLEDGMENTS

The authors gratefully acknowledge very encouraging discussions with Professor A. D. Kent. This paper resulted from a collaboration partially funded by the RTN network ''Computational Magnetoelectronics'' (Contract No. HPRN-CT-2000-00143), the National Science Foundation (Grant DMR 0131883), and by the Research and Technological Cooperation Project between Austria and Hungary (Contract No. A-23/01). Financial support was also provided by the Center for Computational Materials Science (Contract No. GZ 45.451), and the Hungarian National Scientific Research Foundation (OTKA T038162 and OTKA T037856).

[1] A.D. Kent, J. Yu, U. Rüdiger, and S.S.P. Parkin, J. Phys.: Condens. Matter **13**, R461 (2001).
[2] U. Rüdiger, J. Yu, S. Zhang, and A.D. Kent, Phys. Rev. Lett. **80**, 5639 (1998).
[3] T. Nagahama, K. Mibu, and T. Shinjo, J. Appl. Phys. **87**, 5648 (2000).
[4] J.L. Tsai, S.F. Lee, Y.D. Yao, and C. Yu, J. Appl. Phys. **91**, 7983 (2002).
[5] K. Miyake, K. Shigeto, K. Mibu, and T. Shinjo, J. Appl. Phys. **91**, 3468 (2002).
[6] Y.B. Xu, C.A. Vaz, A. Hirohata, H.T. Leung, C.C. Yao, J.A.C. Bland, E. Cambril, F. Rousseaux, and H. Launois, Phys. Rev. B **61**, R14 901 (2000).
[7] A. Hirohata, Y.B. Xu, C.C. Yao, H.T. Leung, W.Y. Lee, S.M. Gardiner, D.G. Hasko, and J.A.C. Bland, J. Appl. Phys. **87**, 4227 (2000).
[8] A. Hirohata, Y.B. Xu, C.C. Yao, H.T. Leung, W.Y. Lee, S.M. Gardiner, D.G. Hasko, J.A.C. Bland, and S.N. Holmes, J. Magn. Magn. Mater. **226-230**, 1845 (2001).
[9] J.L. Tsai, S.F. Lee, Y.D. Yao, and C. Yu, J. Magn. Magn. Mater. **239**, 246 (2002).
[10] J. Schwitalla, B.L. Györffy, and L. Szunyogh, Phys. Rev. B **63**, 104423 (2001).
[11] P. Weinberger, and L. Szunyogh, Comput. Phys. Commun. **17**, 414 (2000).

[12] P. Weinberger, P.M. Levy, J. Banhart, L. Szunyogh, and B. Újfalussy, J. Phys.: Condens. Matter **8**, 7677 (1996).
[13] P. Weinberger, Philos. Mag. B **75**, 509 (1997).
[14] P. Weinberger, L. Szunyogh, C. Blaas, C. Sommers, and P. Entel, Phys. Rev. B **63**, 094417 (2001).
[15] P. Weinberger, Phys. Rep. **377**, 281 (2003).
[16] C. Blaas, L. Szunyogh, P. Weinberger, C. Sommers, and P.M. Levy, Phys. Rev. B **63**, 224408 (2001).
[17] S. Khmelevskyi, K. Palotás, L. Szunyogh, and P. Weinberger, Phys. Rev. B **68**, 012402 (2003).
[18] C.L. Comstock, *Introduction to Magnetism and Magnetic Recording* (Wiley, New York, 1999), pp. 205 and 206.